The enhancement of neutron rich particle emission from out-fission-plane in Fermi energy heavy ion reactions

Yijie Wang,[1,*] Sheng Xiao,[1] Mengting Wan,[2,3] Xinyue Diao,[1] Yuhao Qin,[1] Zhi Qin,[1] Dong Guo,[1] Dawei Si,[1] Boyuan Zhang,[1] Baiting Tian,[1] Junhuai Xu,[1] Fenhai Guan,[1] Qianghua Wu,[1] Xianglun Wei,[4] Herun Yang,[4] Peng Ma,[4] Rongjiang Hu,[4] Limin Duan,[4] Fangfang Duan,[4] Junbing Ma,[4] Shiwei Xu,[4] Qiang Hu,[4] Zhen Bai,[4] Yanyun Yang,[4] Jiansong Wang,[4,5] Wenbo Liu,[6] Wanqing Su,[6] Xiaobao Wei,[6] Chun-Wang Ma,[6] Xinxiang Li,[7,8] Hongwei Wang,[8,9] Yingxun Zhang,[10] Michał Warda,[11] Arthur Dobrowolski,[11] Bożena Nerlo-Pomorska,[11] Krzysztof Pomorski,[11] Li Ou,[2,3,†] and Zhigang Xiao[1,12,‡]

[1]Department of Physics, Tsinghua University, Beijing 100084, China
[2]College of Physics and Technology, Guangxi Normal University, Guilin 541004, China
[3]Guangxi Key Laboratory of Nuclear Physics and Technology, Guangxi Normal University, Guilin 541004, China
[4] Institute of Modern Physics, Chinese Academy of Sciences, Lanzhou 730000, China
[5] School of Science, Huzhou University, Huzhou, 313000, China;
[6]Institute of Particle and Nuclear Physics, Henan Normal University, Xinxiang 453007, China
[7]School of Nuclear Science and Technology, University of South China, Hengyang 421001, China
[8]Shanghai Institute of Applied Physics, Chinese Academy of Science, Shanghai 201800, China
[9]Shanghai Advanced Research Institute, Chinese Academy of Science, Shanghai 201210, China
[10]China Institute of Atomic Energy, Beijing 102413, China
[11]Institute of Physics, Maria Curie Skłodowska University, 20-031 Lublin, Poland
[12]Collaborative Innovation Center of Quantum Matter, Tsinghua University, Beijing 100084, China

(Dated: September 14, 2024)

The neutron richness of the light charged particles emitted out of the fission plane in heavy ion reactions has been experimentally investigated via the production of $A = 3$ mirror nuclei in ^{86}Kr +$^{\rm nat}$Pb reactions at 25 MeV/u. The energy spectra and angular distributions of triton (t) and ^{3}He in coincidence with two fission fragments are measured with the Compact Spectrometer for Heavy IoN Experiment (CSHINE) and compared to the simulations using the improved quantum molecular dynamics model (ImQMD05). The energy spectrum of ^{3}He is observed harder than that of triton in the fission events, in accordance with the phenomena reported as "^{3}He-puzzle" in inclusive measurements. It is observed that the yield ratio R(t/^{3}He) increases with the angle to the fission plane, in qualitative agreement with the transport model simulations. The enhancement R(t/^{3}He) out of fission plane supports the neutron rich feature of neck emission and provides a novel probe for the nuclear symmetry energy.

PACS numbers:

I. INTRODUCTION

Heavy ion reactions (HIR) provide a femtoscopic laboratory for investigating the properties of the nuclear equation of state (nEoS), particularly the nuclear symmetry energy $E_{\rm sym}(\rho)$ [1–6]. The stringent constraint of $E_{\rm sym}(\rho)$ is crucial for both nuclear- and astro-physics, and draws the most attention since the detection of the gravitational waves from the neutron star merging event GW170817 [7–9]. Although great progress has been made via the detection of isobaric yield ratios in HIRs, like n/p [10], t/^{3}He [11, 12], π^-/π^+ [13–16], K^0/K^+ [17] and Ξ^-/Ξ^0 [18], the $E_{\rm sym}(\rho)$ is still suffering a lot uncertainties [19–23], and the efforts are ongoing to search novel probes to explore the effects of $E_{\rm sym}(\rho)$ in HIRs [24–27].

The nuclear (fast)fission process is a large-amplitude collective motion mode happening in the HIRs. The low-density neutron rich neck region formed in the rupture of two fission fragments provides a good condition for studying $E_{\rm sym}(\rho)$ and dynamic properties in isospin degree of freedom (IDOF)[28–31]. The neck zone has been explored to understand the mechanism of intermediate mass fragment (IMF) formation [32–35], isotopic cluster emission [36–39] and neutron-proton equilibration [40–44]. Because of the density gradient and the isospin migration, the neck zone provides a beneficial environment to study the $E_{\rm sym}(\rho)$ [42, 44]. For more discussions about neck zone, one can refer to the review articles of heavy ion reactions from the experimental [28, 29, 45] and theoretic points of view [46–50].

The emissions of light particles in coincidence with fission fragments is a natural idea for exploring the symmetry energy effect and (fast)fission properties in HIRs [30, 31]. Among the probes using the light charged particles (LCPs), the yield ratio of t/^{3}He, written as R(t/^{3}He), has been particularly identified to probe the enriched feature of isospin dynamics in HIRs. Transport model calculations demonstrate that the R(t/^{3}He) at intermediate-energy HIRs depends on the stiffness of $E_{\rm sym}(\rho)$ [12, 51]. At high-energy HIRs, R(t/^{3}He) depends more sensitively on the value of $E_{\rm sym}(\rho)$ [52] and the specific form of the interaction potential [16, 53], but is less dependent on the slope of $E_{\rm sym}(\rho)$ [54]. In addition, R(t/^{3}He) reflects the isospin dependent nucleon density in the reactions [33, 55, 56]. Experimentally, the yield ratios of various mirror nucleus pairs, including the R(t/^{3}He), led to the discovery of isospin fractionation [57]. It has been suggested that more neutron-rich particles are emitted at midrapidity, as inferred by the $R(t/^3He)$, which correlates positively with the charge number of projectile-like fragments[33] but reversely with the center of mass energy [58]. Similarly, in high-energies HIR, the $R(t/^3He)$ reflects the neutron enrichment of the emission source[33, 59, 60] and isospin mixing during the collision [61]. Recently, the $R(t/^3He)$ has also been used to study the pick-up mechanism of pre-equilibrium light nucleus production in the pion scattering experiment [62]. Hence, the distribution of $R(t/^3He)$ relative to the fission plane is a good prob to characterize the properties of fission process and explore the properties of symmetry energy.

Despite of the enormous progress of the studies on the triton (t) and ^{3}He emission, some questions remain unclear and require further studies. For example, when considering the spectra of ^{3}He, there is an anomalous phenomenon that the yield of high energy ^{3}He is relatively larger, compared to that of triton [63–67] or ^{4}He [63, 65–68]. This phenomenon has been called "^{3}He-puzzle" [63, 64, 67]. While the energy spectra are suffering "^{3}He-puzzle", the yield ratio of triton and ^{3}He is sensitive to the neutron-to-proton ratio (N/Z) of the emitting system [43, 60, 69, 70]. The excitation function of $R(t/^3He)$ measured by the FOPI collaboration [71] can not be reproduced with a single model [52]. More interestingly, the results of the INDRA experiment suggest that the triton and ^{3}He isobars seem to dominate the neutron enrichment of the neck zone [44]. However, the existence of "^{3}He-puzzle" in the coincidence events of LCPs and fission fragments is still an uncertain issue.

Due to the enriched but not-well-understood information carried by triton and ^{3}He coupling to both the isospin transport and the neck emission during fission process in HIRs, we are motivated to explore the emission of these two isobars in coincidence with fission fragments by inspecting the energy spectra and the yield ratio $R(t/^3He)$ over wide angular range, and to bridge the ratio $R(t/^3He)$ and the feature of fission process. In this article, the energy spectra of triton and ^{3}He in coincidence with fission fragments at different angles are measured in the reactions of ^{86}Kr+^{nat}Pb at 25 MeV/u. The distributions of $R(t/^3He)$ with respect to the fission plane and as a function of the laboratory polar angle are analyzed. The comparison of the experimental data to the transport model simulation is discussed. The paper is organized as following. Section 2 and 3 present the experimental setup and the description of the transport model, respectively. Section 4 is the results and the discussions, and section 5 is the summary.

II. EXPERIMENTAL SETUP

The experiment was conducted at the Compact Spectrometer for Heavy IoN Experiment (CSHINE) [72, 73], built at the final focal plane of the Radioactive Ion Beam Line at Lanzhou (RIBLL-I) [74]. The ^{86}Kr beam of 25 MeV/u was extracted from the cyclotron of the Heavy Ion Research Facility at Lanzhou (HIRFL) [75], bombarding a natural lead target installed in the scattering chamber with the radius $R \approx 750$

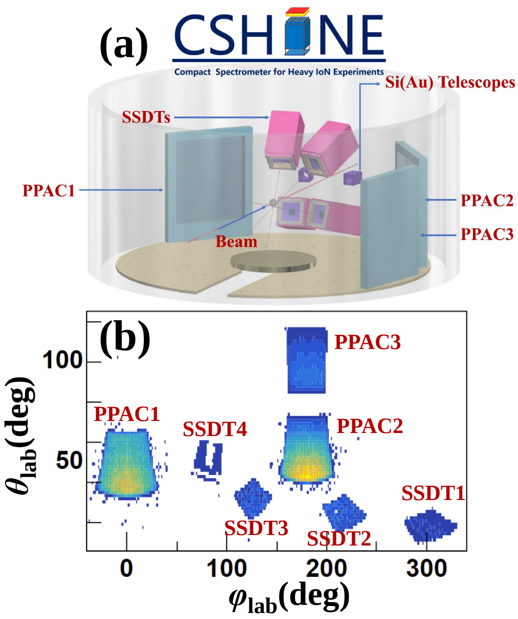

FIG. 1: (Color online) (a) The experimental setup of CSHINE. (b) The spatial coverage of SSDTs and PPACs on $\theta - \varphi$ plane in laboratory reference frame.

mm. The target thickness is about 1 mg/cm^2. Fig. 1 presents the experimental setup (a) and the spatial coverage of the silicon-strip detector telescopes (SSDTs) and the parallel plate avalanche counters (PPACs) (b).

The LCPs from the reactions were measured by 4 SSDTs, covering the angular range from 10° to 60° in laboratory. Each SSDT consists of three layers, namely, one single-sided silicon-strip detector (SSSSD) for ΔE_1 and one double-sided silicon strip detector (DSSSD) for ΔE_2, backed by a 3×3 CsI(Tl) crystal hodoscope with the length of 50 mm for the energy deposit E. The granularity of the SSDT is 4×4 mm^2, giving about 1° angular resolution. The energy resolution of the SSDT is better than 2%, and the isotopes up to $Z = 6$ can be identified [27]. Multi hits and signal sharing are carefully treated in the track recognition, and the track recognition efficiency is about 90% [76]. Fig. 2 shows the particle identification of light particles for this analysis. Panel (a) to (d) presents the scattering plot of $\Delta E_2 - E_{CsI}$ of the four SSDTs. The results show that $Z \leq 3$ LCPs, including triton and ^{3}He, were identified clearly in each SSDT, supporting the reliability of the experimental results.

In order to explore the isospin properties of fission process, the fission fragments (FFs) were detected by 3 PPACs, each of which had a sensitive area of 240×280 mm^2 [77, 78]. The perpendicular distance of the PPACs to the target is about 428 mm. The coverage of the PPACs ensures a high efficiency to measure the FFs in coincidence with the LCPs. And the trigger system is established to selected the fission events [79]. The working voltage of the PPACs can suppress the light charged particles significantly. According to the previous source test results [72], the detection efficiency is almost

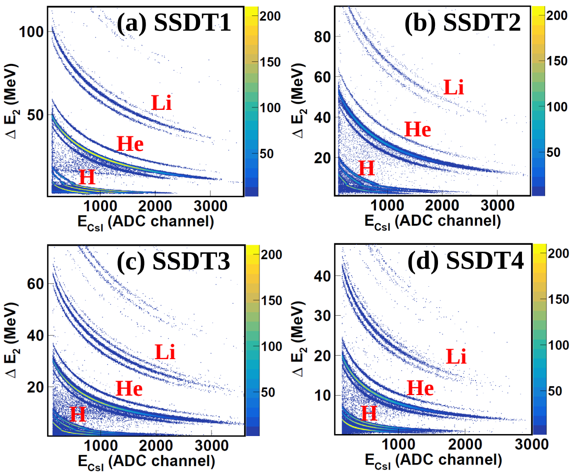

FIG. 2: (Color online) $\Delta E_2 - E_{\mathrm{CsI}}$ plots of the four SSDTs.

100% for FFs and negligibly low for light particles with the detector condition (HV=460 V) as adopted in the experiment. So, the PPACs can only be fired by heavy fragments, rather than LCPs or IMFs.

Referring to the energy loss calculations only, the projectile-like fragments (PLF) and target-like fragments (TLF) may fire the PPACs as well. However, the geometric coverage of the PPACs in the experiment suppresses the PLF and TLF. Otherwise because PLFs and TLFs are well separated in velocity ($v_{\mathrm{PLF}} = 6.8$ cm/ns, $v_{\mathrm{TLF}} = 1.2$ cm/ns at linear momentum transfer LMT = 0.5), one shall be able to see two components clearly on the velocities of the two coincident fragments recorded in the PPACs. On the contrary, the two-component feature is not visible in the velocity scattering plot [77]. Hence, it is safe and reasonable to speculate that the heavy fragments detected with PPACs in the experiment are fission fragments.

III. THEORETICAL MODEL

A hybrid model by the improved quantum molecular dynamics model (ImQMD05) coupled with statistical decay afterburner (GEMINI) was used for theoretical simulation in this work. The ImQMD05 [80] was used to simulate the nucleon transport process in HIRs. And the GEMINI [81, 82] was appended to obtain the final state productions of the reactions. The ImQMD05 model is an improved version from the original quantum molecular dynamics code [83, 84], and is widely used to understand the dynamics of nuclear reactions induced by heavy ions or light nuclei at both low and intermediate energies [30, 31, 85–87] . The mean field part of the ImQMD05 model used here includes the symmetry potential energy part. And the local nuclear potential energy density functional in the ImQMD05 model is written as

$$V_{\mathrm{loc}} = \frac{\alpha}{2}\frac{\rho^2}{\rho_0} + \frac{\beta}{\eta+1}\frac{\rho^{\eta+1}}{\rho_0^{\eta}} + \frac{g_{\mathrm{sur}}}{2\rho_0}(\nabla\rho)^2 + \frac{g_{\mathrm{sur,iso}}}{\rho_0}[\nabla(\rho_{\mathrm{n}}-\rho_{\mathrm{p}})]^2 + g_{\rho\tau}\frac{\rho^{8/3}}{\rho_0^{5/3}} + \frac{C_{\mathrm{s}}}{2}\frac{\rho^{\gamma+1}}{\rho_0^{\gamma}}\delta^2, \qquad (1)$$

where ρ, ρ_{n} and ρ_{p} are the density of nucleon, neutron and proton, respectively. $\delta = (\rho_{\mathrm{n}} - \rho_{\mathrm{p}})/(\rho_{\mathrm{n}} + \rho_{\mathrm{p}})$ is the isospin asymmetry degree. The parameters in Eq. (1) except C_{s}, which are listed in Table I, are obtained directly from Skyrme interaction with MSL0 parameter set [88]. C_{s} is determined by the symmetry potential energy at saturation density. Together with different values of γ, one can get the MSL0-like Skyrme interaction with various density dependent symmetry potential energy. The reaction was simulated with impact parameter in the range of $1.0 \le b \le 7.0$ fm by step of $\Delta b = 1.5$ fm. At the end of the dynamical evolution in ImQMD05, the minimum spanning tree (MST) algorithm [84, 89] was used to recognize the free nucleons and fragments formed in the evolution. Next, the statistical decay of excited fragments was performed with GEMINI afterburner. At last, the information of final state particles will be obtained.

IV. RESULTS AND DISCUSSIONS

A. Characterizing the fission events

We start with the analysis of the orientation of the fission plane with respect to the beam direction. The fission plane is reconstructed by the velocity of two FFs, using $\vec{n}_{\mathrm{FF}} = (\vec{v}_{\mathrm{F}_1} \times \vec{v}_{\mathrm{F}_2}) / |\vec{v}_{\mathrm{F}_1}||\vec{v}_{\mathrm{F}_2}|$ to denote the normal vector of the fission plane, as shown in Fig. 3 (a). Defining α_1 as the angle between $\vec{n}_{\mathrm{FF}}$ and the beam direction $\vec{v}_{\mathrm{beam}}$, one can characterize how much the fission plane deviates from the beam. The distribution of $|\cos(\alpha_1)|$ is peaked at 0 with a rather small width $\sigma_{\alpha_1} \approx 6^\circ$, as shown in Fig. 3(b), inferring that the fission plane keeps approximately the memory of the initial angular momentum of the rotating system. The transport model prediction about the distribution of $|\cos(\alpha_1)|$ is in rather agreement with the experiment. The scattering plots of folding angle *vs.* $|\cos(\alpha_1)|$ provide the information of fission and detection geometry. With the detector filter of PPACs on both θ_{lab} and ϕ_{lab} according to the experiment setup, the experimental folding angle in Fig. 3(c) can be approximately described by the model simulation in Fig. 3(d).

The characteristics of this rotating fission system was estimated with the experiment data and theory calculation results. First, to estimate the charge and mass of the rotating fission system, the linear momentum transfer (LMT) should be estimated experimentally. Assuming a symmetric fission processes, the velocity of the fissioning system (FS) can be simply calculated by

TABLE I: Parameter set used in the ImQMD05 calculations.

α (MeV)	β (MeV)	η	g_{sur} (MeV fm^2)	$g_{\mathrm{sur,iso}}$ (fm^2)	$g_{\rho\tau}$ (MeV)	C_s (MeV)	ρ_0 (fm^{-3})
-254	185	5/3	21.0	-0.82	5.51	36.0	0.160

$$\vec{v}_{\mathrm{FS}} = \frac{1}{2}(\vec{v}_{\mathrm{F1}} + \vec{v}_{\mathrm{F2}}), \quad (2)$$

where $\vec{v}_{\mathrm{F1}}$ and $\vec{v}_{\mathrm{F2}}$ are the velocities of the two FFs, respectively. And the velocity of system in beam direction is labeled as v^Z_{FS} .

The LMT is defined as

$$\mathrm{LMT} = \frac{A_{\mathrm{tar}} \times v^Z_{\mathrm{FS}}}{A_{\mathrm{pro}} \times (v_{\mathrm{pro}} - v^Z_{\mathrm{FS}})}, \quad (3)$$

Here the subscripts *pro* and *tar* denotes the projectile and the target, respectively. In Fig. 4, the distribution of the LMT derived from the experimental data is peaked in the vicinity of 0.4. The small peak below LMT < 0.2 is contributed by the fission events triggered by PPAC 1 and PPAC 3. Accordingly, the typical charge and mass of the rotating fission system are $Z_{\mathrm{FS}} \approx Z_{\mathrm{tar}} + (Z_{\mathrm{pro}} \times \mathrm{LMT}) = 96$ and $A_{\mathrm{FS}} \approx A_{\mathrm{tar}} + (A_{\mathrm{pro}} \times \mathrm{LMT}) = 242$.

Second, to estimate the angular momentum of the rotating fission system, one needs the most probable impact parameter, which can determined by the event weigh obtained from transport model simulations filtered by experimental conditions. Defining the fission event weight by

$$W_{\mathrm{F}} = b \times \frac{n_{\mathrm{F}}}{N_{\mathrm{tot}}(b)}, \quad (4)$$

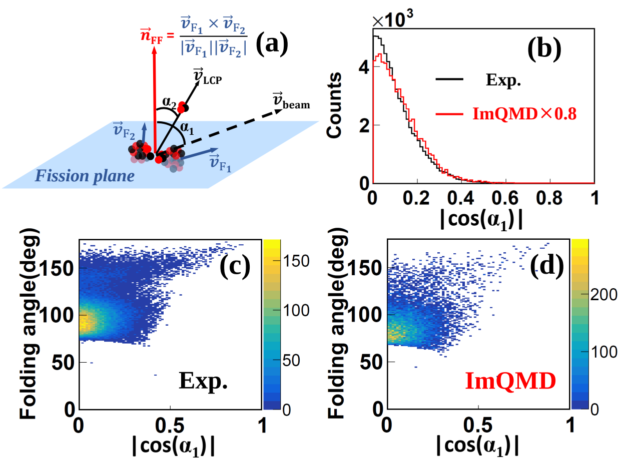

FIG. 3: (Color online) (a) Geometric diagram of fission plane of FFs and LCP emission. (b) Angular distribution between the normal vector $\vec{n}_{\mathrm{FF}}$ of the fission plane and the beam direction $\vec{v}_{\mathrm{beam}}$. The experimental (c) and simulation (d) results of the folding angle *vs.* $|\cos(\alpha_1)|$.

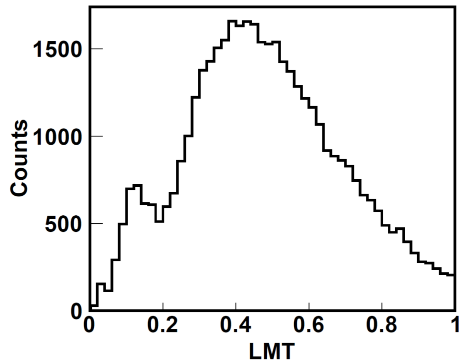

FIG. 4: (Color online) Experimental distribution of LMT.

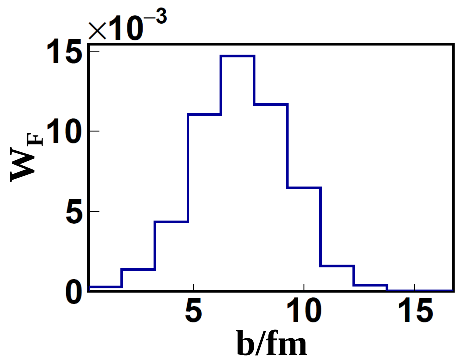

FIG. 5: (Color online) The weight of the fission events as a function of impact parameter b in ImQMD05 simulations.

where n_{F} is the number of fission events counted in N_{tot} events simulated at a given impact parameter b.

Fig. 5 shows the distribution of W_{F}, where the most probable impact parameter b_{m} is located in the vicinity of 7 fm.

The distance between the transferred part of the projectile and the mass center of the fissioning system is defined as

$$D = b_{\mathrm{m}} \frac{A_{\mathrm{tar}}}{A_{\mathrm{tar}} + (A_{\mathrm{pro}} \times \mathrm{LMT})}, \quad (5)$$

where $b_{\mathrm{m}} = 7$ fm, $A_{\mathrm{tar}} = 208$, $A_{\mathrm{pro}} = 86$ and LMT $= 0.4$, respectively.

And the angular momentum is written as

$$J = P_{\mathrm{pro}} \times \mathrm{LMT} \times D, \quad (6)$$

where $P_{\mathrm{pro}} = 18700$ MeV/c and $D = 6$ fm was derived with LMT $= 0.4$. Then, the angular momentum of the rotating system is approximately $J \approx 200\ \hbar$.

Third, to estimate the excitation energy of the rotating fission system, we regard the fissioning system as in sphere shape, and calculate its moment of inertia as

$$I = \frac{2}{5} A_{\rm FS} r_{\rm FS}^2, \tag{7}$$

where $r_{\rm FS} = 1.4 A_{\rm FS}^{1/3}$ is the radius of the fissioning system. The rotating energy $E_{\rm rot} = J^2/2I \approx 100$ MeV is approximately obtained. Ignoring the reaction Q value, the excitation energy could be extracted by

$$E^* = E_{\rm kin}^{\rm i} - E_{\rm kin}^{\rm f} - E_{\rm rot}, \tag{8}$$

where $E_{\rm kin}^{\rm i}$ and $E_{\rm kin}^{\rm f}$ are the initial state kinetic energy and the final state kinetic energy, respectively. Approximately, one has $E^* \approx 600$ MeV. The excitation energy is close to the one of the fission system formed in 25 MeV/u Ar+Au at LMT ≈ 80%, where the E^* was calculated by the pre scission α multiplicity [90].

B. Analysis of the energy spectra of t and ^{3}He

We now present the analysis of the emission of triton and ^{3}He in the (fast)fission events. The energy spectra of LCPs in coincidence with FFs contain thermal and dynamical information of the particles emitted from the fission events. Fig. 6 presents the energy spectra of triton (open circles) and ^{3}He (open triangles) emitted from fission events in different angular ranges corresponding to SSDTs 2 to 4. To reduce the contamination of quasi-projectiles, the data of SSDT1 covering 10 – 20° in the laboratory is not counted here. It is shown that the spectrum of ^{3}He is generally harder than that of triton, leading to a larger average kinetic energy of the former. The difference between triton and ^{3}He is more pronounced at forward angles than at large angles. This observation of "^{3}He-puzzle" is in accordance with the previous inclusive measurements at high beam energies [63, 65–67, 71, 91–94].

The "^{3}He-puzzle" has been interpreted by two possible scenarios: sequential decay [64] and coalescence model [68]. In the sequential decay scenario, the difference between ^{3}He and triton is influenced by the Coulomb barrier, for which ^{3}He is emitted at an earlier stage with high temperature to overcome the Coulomb barrier higher than that of triton [64]. In coalescence scenario, which was applied to interpret the difference between ^{3}He and α particles [68], the former is dominantly produced by the coalescence of preequilibrium nucleons, delivering larger mean kinetic energy. These two explanations are qualitatively in agreement, supporting that ^{3}He is predominantly emitted at earlier stage. Our experimental results show that the "^{3}He-puzzle" exists in the events tagged by fission. It suggests that the puzzle exists in both inclusive and fission events.

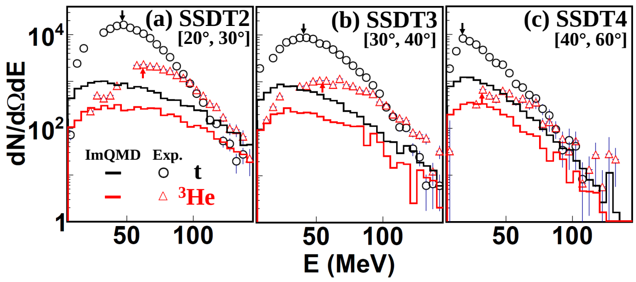

FIG. 6: (Color online) The experimental energy spectra of triton (circle) and ^{3}He (triangle) in $20° \leq \theta_{\rm lab} \leq 60°$ covered by SSDT2 to SSDT4 in coincidence with two FFs. The arrows represent the peak position of each experimental energy spectrum. The theoretical energy spectra from coincident events of one LCP and two FFs (Z≥10) with the same angular cuts as experiment results are drawn with black (triton) and red (^{3}He) lines.

TABLE II: Energy peak position $E_{\rm p}$ of triton and ^{3}He for SSDT 2 to 4.

	SSDT2	SSDT3	SSDT4
$E_{\rm p}$ of triton (MeV)	45	40	19
$E_{\rm p}$ of ^{3}He (MeV)	62	58	38

The energy spectra calculated by ImQMD05 are presented in Fig. 6 with black and red lines for triton and ^{3}He, respectively. The coincident events of one LCP and two FFs with the same detection geometry cuts as experimental results are analyzed. In order to gain statistics and save CPU time in simulations, the cut to identify a fission fragment is loosen to $Z \geq 10$, which is quite small but does not influence the conclusion. It can be seen that the trend of the spectra of triton and ^{3}He is qualitatively repeated by the model calculations. Switching from triton to ^{3}He, the energy spectra become slightly harder, and the energy peak positions move to the high energy side, less pronounced in comparison with the data. At large angles, as shown in panel (b) and (c), the simulated descending tails of ^{3}He spectra agree better with the experiment data compared to that of triton, suggesting that the high-energy ^{3}He is dominated by dynamic emissions. Quantitatively speaking, however, the splitting between triton and ^{3}He in model calculations is less pronounced than in the experimental data, particularly at smaller angles. It suggests that the origin and the formation of light clusters, as of triton and ^{3}He, is seemingly more complicated than the cluster formation approach usually adopted by current transport models.

C. Out-plane emission and the effect of $E_{\rm sym}(\rho)$

Benefiting from the wide angular coverage of the SSDTs and PPACs in laboratory reference frame, the angular behavior of the particle emission can be analyzed. To avoid the influence of the possible experimental distortion caused by the energy threshold in each SSDTs, we focus on the descending

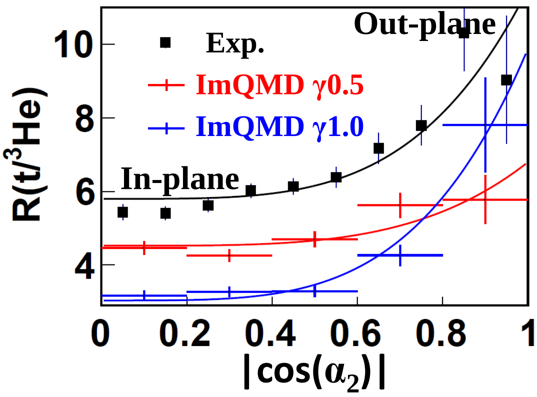

FIG. 7: (Color online) The ratio $R(\mathrm{t}/^3\mathrm{He})$ as a function of $|\cos(\alpha_2)|$. The black solid squares and black line represent the experiment data and fitting result. The red and blue cross markers (lines) represent the theoretical calculations data (fitting results) of $\gamma = 0.5$ and 1.0.

part on the high energy side of the energy peak. The energy peak positions (E_p) are listed in Table II. Meanwhile, using the energy condition $E \geq E_\mathrm{p}$ as the low limit cut, one can suppress the interference of the evaporation process and emphasize the feature of the dynamic emission.

Fig. 7 presents the angular distribution of $R(\mathrm{t}/^3\mathrm{He})$ with respect to the fission plane. The α_2 on the abscissa is the relative angle between $\vec{n}_\mathrm{FF}$ and the velocity of the coincident triton or ^{3}He $\vec{v}_\mathrm{LCP}$ (shown in Fig. 3 (a)), with $|\cos(\alpha_2)| = 0$ (1) corresponding to in-plane (out-plane) emission. Again, the same cuts are applied for both experimental and theoretical results. The increasing trend of $R(\mathrm{t}/^3\mathrm{He})$ with $|\cos(\alpha_2)|$ indicates that the neutron rich particles emitted from out-fission-plane is enhanced. This phenomenon is the consequence of the competition between the isospin migration and the centrifugal motion of the particles in the rotating fission system. When the reaction system is viewed as a rotating emission source, particles emitted near the fission plane are subjected to stronger centrifugal potential during the emission process, weakening the difference between neutrons and protons under the isovector potential. From the in-plane to out-plane, more neutron rich particles are emitted due to the effect of isospin fractionation [57], indicating that the effect of the isovector potential becomes more significant compared to centrifugal potential. This observation gives us the chance to explore the properties of isospin transport and the density dependence of $E_\mathrm{sym}(\rho)$ in (fast)fission reactions.

In order to see the symmetry energy effect, a soft ($\gamma = 0.5$) and a stiff ($\gamma = 1.0$) symmetry energy are adopted in the ImQMD05 simulations. These two γ values correspond to slope parameter range $51 < L < 77$MeV at saturation density ρ_0. To describe the increasing trend of the angular distribution of $|\cos(\alpha_2)|$, the function of $f(x) = p_0 + p_1 x^4$ is used to fit data. Here p_0 reflects the overall ratio of $R(\mathrm{t}/^3\mathrm{He})$, which is far off to the experiment due to the clustering difficulty of transport model. However, the parameter p_1 can be used to describe the increasing rate of the ratio with out-of-plane angle. In Fig. 7,

TABLE III: Fitting results of $R(\mathrm{t}/^3\mathrm{He})$ as a function of $|\cos(\alpha_2)|$ using $f(x) = p_0 + p_1 x^4$.

	p₀	p₁
Experiment	5.8±0.2	5.7±1.6
γ=0.5	4.5±0.1	2.3±1.1
γ=1.0	3.0±0.1	6.8±1.8

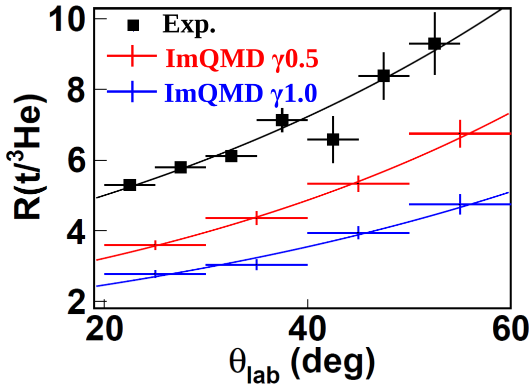

FIG. 8: (Color online) The ratio $R(\mathrm{t}/^3\mathrm{He})$ as a function of θ_lab. The black solid squares and black line represent the experiment data and fitting result with $E \geq E_\mathrm{p}$ cuts in coincidence with fission events. The red and blue cross markers (lines) represent the ImQMD05 calculations data (fitting results) of $\gamma = 0.5$ and 1.0.

the theoretical fitting lines shows a different increasing behavior between $\gamma = 0.5$ and 1.0, indicating that the enhancement of neutron rich particle emission out of fission plane is sensitive to the form of $E_\mathrm{sym}(\rho)$. Inspecting the increasing curves and the values of p_1 as listed in Table III, one finds that the experimental increasing rate situates between the theoretical prediction with $\gamma = 0.5$ and 1.0, in accordance with the conclusion of our previous work [27], where a totally different probe was used. The comparison seems to exclude very soft (γ <0.5) and very stiff (γ >1.0) candidates of symmetry energy. The results indicate that the ratio $R(\mathrm{t}/^3\mathrm{He})$ as a function of $|\cos(\alpha_2)|$ is a sensitive probe for density dependent symmetry energy, especially in the larger $|\cos(\alpha_2)|$ range, which is very close to the boundary of the detector coverage. Hence, more events in the larger $|\cos(\alpha_2)|$ range are preferentially requested in the further experimental measurements.

Furthermore, the angular distribution of $R(\mathrm{t}/^3\mathrm{He})$ as a function of the polar angle in laboratory θ_lab is generated with events of one LCP in coincidence with two FFs, as shown in Fig. 8. The same energy threshold, geometry and folding angle cuts are applied to both experimental and simulation results. It is shown that for the wide angular range, the distribution exhibits a rising trend. This feature is consistent with the moving source picture, where the neutron richness of particle emission increases from the projectile-like source to the medium velocity source corresponding to the neck, as predicted by various transport model simulations [30, 31, 36, 38, 39, 41, 95–99], and experimentally observed

TABLE IV: Fitting results of the ratio $R(\mathrm{t}/^{3}\mathrm{He})$ as a function of θ_{lab} using $f(x) = \exp(p_0 + p_1 x)$

	p_0	p_1
Experiment	1.24±0.06	0.018±0.002
γ=0.5	0.75±0.08	0.021±0.002
γ=1.0	0.54±0.09	0.018±0.002

in a specific angular window [32, 35, 40, 44, 69, 100–102] or a parallel velocity window [35, 69, 70, 103–108]. The rising trend of $R(\mathrm{t}/^{3}\mathrm{He})$ as a function of θ_{lab} was compared to the ImQMD05 simulation with $\gamma = 0.5$ and 1. The function of $f(x) = \exp(p_0 + p_1 x)$ is applied to fit the data with p_1 inferring the increasing rate of $R(\mathrm{t}/^{3}\mathrm{He})$ to θ_{lab}. Fig. 8 shows that the rising trend depends on γ. Visibly, a softer $E_{\mathrm{sym}}(\rho)$ causes a relative larger increasing rate. When comparing the fitting results between experiment and model in Table IV, the value of experimental p_1 is marginally located between $\gamma = 0.5$ and 1.0. Nevertheless, the large uncertainty here reduces the sensitivity and hinder to make a convincing constraint of $E_{\mathrm{sym}}(\rho)$, compared to the effectiveness of the ratio $R(\mathrm{t}/^{3}\mathrm{He})$ as a function of $|\cos(\alpha_2)|$.

Fig. 9 shows supplementarily the relationship between $|\cos(\alpha_2)|$ and θ_{lab} with the experiment events of triton in coincidence with two fission fragments. Visibly, there is a weak positive correlation between $|\cos(\alpha_2)|$ and θ_{lab}. The origin of the correlation is partly due to the fact that the azimuth coverage of the PPAC is quite limited. With such weak correlation, one infers that the two distributions shown in Fig. 7 and Fig. 8 have their own implications. Namely, the distribution of $R(\mathrm{t}/^{3}\mathrm{He})$ as a function of θ_{lab} indicates that the low density and neutron rich medium velocity emission source (neck) is formed, while the distribution of $R(\mathrm{t}/^{3}\mathrm{He})$ as a function of $|\cos(\alpha_2)|$ characterizes the fine out-plane properties of the isospin transport in a fissioning process. Upon comparing the results presented in Table III and Table IV, it becomes evident that the enhancement of $R(\mathrm{t}/^{3}\mathrm{He})$ *vs.* $|\cos(\alpha_2)|$, particularly at larger out-plane angles, appears to be a more sensitive probe for studying nuclear symmetry energy than the polar angular distribution of $R(\mathrm{t}/^{3}\mathrm{He})$. In another word, in a properly characterized fission events, the effect of $E_{\mathrm{sym}}(\rho)$ can be magnified, confirming the previous predictions by transport model simulations [30].

V. SUMMARY

The energy spectra and angular distributions of triton and ^{3}He ranging from 20° to 60° in the laboratory in coincidence with fission fragments are analyzed in 25 MeV/u ^{86}Kr +$^{\mathrm{nat}}$Pb reactions. It is shown that the energy spectra of ^{3}He are generally harder than triton even in the fission events, and the effect is more pronounced at small angles. The yield ratio $R(\mathrm{t}/^{3}\mathrm{He})$ exhibits an enhancement as a function of $|\cos(\alpha_2)|$, evidencing more neutron rich particles emitted from out-fission-plane.

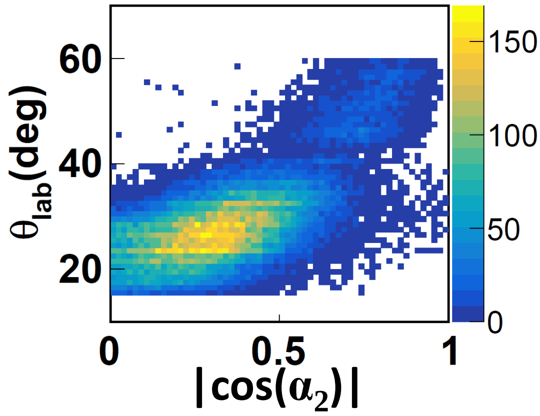

FIG. 9: (Color online) The scattering plot between $|\cos(\alpha_2)|$ and laboratory angle with the experiment events of triton in coincidence with two fission fragments.

The rising trend of angular distribution of $R(\mathrm{t}/^{3}\mathrm{He})$ is also observed in the coincident events of one LCP and two FFs, which is consistent with previous inclusive observations. The ImQMD05 simulations achieve a qualitative description of the energy spectra and the angular distributions of triton and ^{3}He, supporting the dynamic feature of the emission of triton and ^{3}He from the fission process. When comparing the experiment data with theoretical calculations, the results show that both the enhancement of $R(\mathrm{t}/^{3}\mathrm{He})$ *vs.* $|\cos(\alpha_2)|$ and the increasing trend of angular distribution of $R(\mathrm{t}/^{3}\mathrm{He})$ are sensitive to nuclear symmetry energy. Particularly, the enhancement behavior of $R(\mathrm{t}/^{3}\mathrm{He})$ at larger out-fission-plane angles, characterized by $|\cos(\alpha_2)|$, seems a novel probe to understand the nuclear symmetry energy and isospin dynamics related to (fast)fission process. From the comparisons of the experimental results to the transport model simulations, the slope parameter L of $E_{\mathrm{sym}}(\rho)$ is inferred in the range of $51 < L < 77$ MeV at ρ_0. More measurements at large out-fission-plane angles are important for stringent constraint of $E_{\mathrm{sym}}(\rho)$.

ACKNOWLEDGEMENT

This work is supported by the National Natural Science Foundation of China under Grant Nos. 12205160, 11961131010, 11961141004, and 11965004, and by the Ministry of Science and Technology of China under Nos. 2022YFE0103400 and 2020YFE0202001, and by the Polish National Science Center under No. 2018/30/Q/ ST2/00185. This work is also supported by Initiative Scientific Research Program and the Center of High Performance Computing of Tsinghua University, and the Heavy Ion Research Facility at Lanzhou (HIRFL). The authors thank Huigan Cheng from SCUT, Zhen Zhang from SYSU and Rui Wang from INFN for their valuable discussions.

* Electronic address: yj-wang15@tsinghua.org.cn
† Electronic address: liou@gxnu.edu.cn
‡ Electronic address: xiaozg@tsinghua.edu.cn

[1] Bao-An Li, Bao-Jun Cai, Wen-Jie Xie, and Nai-Bo Zhang. Progress in Constraining Nuclear Symmetry Energy Using Neutron Star Observables Since GW170817. *Universe*, 7(6):182, 2021.

[2] S. Huth et al. Constraining Neutron-Star Matter with Microscopic and Macroscopic Collisions. *Nature*, 606:276–280, 2022.

[3] Andrew W. Steiner, Madappa Prakash, James M. Lattimer, and Paul J. Ellis. Isospin asymmetry in nuclei and neutron stars. *Phys. Rept.*, 411:325–375, 2005.

[4] M. Oertel, M. Hempel, T. Klähn, and S. Typel. Equations of state for supernovae and compact stars. *Rev. Mod. Phys.*, 89(1):015007, 2017.

[5] Bao-An Li, Angels Ramos, Giuseppe Verde, and Isaac Vidana. Topical issue on nuclear symmetry energy. *Eur. Phys. J. A*, 50:9, 2014.

[6] Bao-An Li, Lie-Wen Chen, and Che Ming Ko. Recent Progress and New Challenges in Isospin Physics with Heavy-Ion Reactions. *Phys. Rept.*, 464:113–281, 2008.

[7] B. P. Abbott et al. GW170817: Observation of Gravitational Waves from a Binary Neutron Star Inspiral. *Phys. Rev. Lett.*, 119(16):161101, 2017.

[8] B. P. Abbott et al. GW170817: Measurements of neutron star radii and equation of state. *Phys. Rev. Lett.*, 121(16):161101, 2018.

[9] Soumi De, Daniel Finstad, James M. Lattimer, Duncan A. Brown, Edo Berger, and Christopher M. Biwer. Tidal Deformabilities and Radii of Neutron Stars from the Observation of GW170817. *Phys. Rev. Lett.*, 121(9):091102, 2018. [Erratum: Phys.Rev.Lett. 121, 259902 (2018)].

[10] Bao-An Li, C. M. Ko, and Zhong-zhou Ren. Equation of state of asymmetric nuclear matter and collisions of neutron rich nuclei. *Phys. Rev. Lett.*, 78:1644, 1997.

[11] Ying-xun Zhang and Zhu-xia Li. Probing the density dependence of the symmetry potential with peripheral heavy-ion collisions. *Phys. Rev. C*, 71:024604, 2005.

[12] Lie-Wen Chen, Che Ming Ko, and Bao-An Li. Light clusters production as a probe to the nuclear symmetry energy. *Phys. Rev. C*, 68:017601, 2003.

[13] Bao-An Li. Probing the high density behavior of nuclear symmetry energy with high-energy heavy ion collisions. *Phys. Rev. Lett.*, 88:192701, 2002.

[14] Zhigang Xiao, Bao-An Li, Lie-Wen Chen, Gao-Chan Yong, and Ming Zhang. Circumstantial Evidence for a Soft Nuclear Symmetry Energy at Suprasaturation Densities. *Phys. Rev. Lett.*, 102:062502, 2009.

[15] J. Estee et al. Probing the Symmetry Energy with the Spectral Pion Ratio. *Phys. Rev. Lett.*, 126(16):162701, 2021.

[16] Qingfeng Li, Zhuxia Li, Sven Soff, Marcus Bleicher, and Horst Stoecker. Probing the density dependence of the symmetry potential at low and high densities. *Phys. Rev. C*, 72:034613, 2005.

[17] G. Ferini, T. Gaitanos, M. Colonna, M. Di Toro, and H. H. Wolter. Isospin effects on sub-threshold kaon production at intermediate energies. *Phys. Rev. Lett.*, 97:202301, 2006.

[18] Gao-Chan Yong, Bao-An Li, Zhi-Gang Xiao, and Zi-Wei Lin. Probing high-density nuclear symmetry energy with Ξ^-/Ξ^0 ratio in heavy-ion collisions at $\sqrt{s_{NN}} \sim 3$ GeV. *Phys. Rev. C*, 106:024902, 2022.

[19] Jun Xu. Transport approaches for the description of intermediate-energy heavy-ion collisions. *Prog. Part. Nucl. Phys.*, 106:312–359, 2019.

[20] Yong-Jia Wang and Qing-Feng Li. Application of microscopic transport model in the study of nuclear equation of state from heavy ion collisions at intermediate energies. *Front. Phys. (Beijing)*, 15(4):44302, 2020.

[21] Ying-Xun Zhang et al. Comparison of heavy-ion transport simulations: Collision integral in a box. *Phys. Rev. C*, 97(3):034625, 2018.

[22] Akira Ono et al. Comparison of heavy-ion transport simulations: Collision integral with pions and Δ resonances in a box. *Phys. Rev. C*, 100(4):044617, 2019.

[23] Maria Colonna et al. Comparison of heavy-ion transport simulations: Mean-field dynamics in a box. *Phys. Rev. C*, 104(2):024603, 2021.

[24] Yan Zhang et al. Long-time drift of the isospin degree of freedom in heavy ion collisions. *Phys. Rev. C*, 95(4):041602, 2017.

[25] Li Ou, Zhigang Xiao, Han Yi, Ning Wang, Min Liu, and Junlong Tian. Dynamic Isovector Reorientation of Deuteron as a Probe to Nuclear Symmetry Energy. *Phys. Rev. Lett.*, 115(21):212501, 2015.

[26] Yijie Wang et al. The emission order of hydrogen isotopes via correlation functions in 30 MeV/u Ar+Au reactions. *Phys. Lett. B*, 825:136856, 2022.

[27] Yijie Wang et al. Observing the ping-pong modality of the isospin degree of freedom in cluster emission from heavy-ion reactions. *Phys. Rev. C*, 107(4):L041601, 2023.

[28] G. Poggi. Neck emissions and the isospin degree of freedom. *Nucl. Phys. A*, 685:296–311, 2001.

[29] M Di Toro, Alessandro Olmi, and R Roy. Neck dynamics. In *Dynamics and Thermodynamics with Nuclear Degrees of Freedom*, pages 65–70. Springer, 2006.

[30] Qianghua Wu, Fenhai Guan, Xinyue Diao, Yijie Wang, Yingxun Zhang, Zhuxia Li, Xizhen Wu, Artur Dobrowolski, Krzysztof Pomorski, and Zhigang Xiao. Symmetry energy effect on emissions of light particles in coincidence with fast fission. *Phys. Lett. B*, 811:135865, 2020.

[31] Qianghua Wu, Xinyue Diao, Fenhai Guan, Yijie Wang, Yingxun Zhang, Zhuxia Li, Xizhen Wu, Krzysztof Pomorski, and Zhigang Xiao. Transport model studies on the fast fission of the target-like fragments in heavy ion collisions. *Phys. Lett. B*, 797:134808, 2019.

[32] J. Toke et al. Intermediate-Mass Fragment Decay of the Neck Zone Formed in Peripheral Bi-209 + Xe-136 Collisions at Elab/A=28 MeV. *Phys. Rev. Lett.*, 75:2920–2923, 1995.

[33] J. F. Dempsey et al. Isospin dependence of intermediate mass fragment production in heavy-ion collisions at E/A=55 MeV. *Phys. Rev. C*, 54:1710–1719, 1996.

[34] E. Ramakrishnan, H. Johnston, F. Gimeno-Nogues, D. J. Rowland, R. Laforest, Y-W. Lui, S. Ferro, S. Vasal, and S. J. Yennello. Fragment emission from the mass-symmetric reactions Fe-58, Ni-58 + Fe-58, Ni-58 at Ebeam= Me-30V/nucleon. *Phys. Rev. C*, 57:1803–1811, 1998.

[35] S. Hudan et al. Comparison of mid-velocity fragment formation with projectile-like decay. *Phys. Rev. C*, 71:054604, 2005.

[36] L. G. Sobotka, J. F. Dempsey, R. J. Charity, and P. Danielewicz. Clustered and neutron-rich low density 'neck' region produced in heavy-ion collisions. *Phys. Rev. C*, 55:2109–2111, 1997.

[37] R. Laforest, E. Ramakrishnan, D. J. Rowland, A. Ruangma, E. M. Winchester, E. Martin, and S. J. Yennello. Depen-

dence of projectile fragmentation on target N/Z. *Phys. Rev. C*, 59:2567–2573, 1999.

[38] YingXun Zhang, ChengShuang Zhou, JiXian Chen, Ning Wang, Kai Zhao, and ZhuXia Li. Correlation between the fragmentation modes and light charged particles emission in heavy ion collisions. *Science China Physics, Mechanics & Astronomy*, 58:1–8, 2015.

[39] Zhao-Qing Feng. Effects of isospin dynamics on neck fragmentation in isotopic nuclear reactions. *Phys. Rev. C*, 94(1):014609, 2016.

[40] A. Rodriguez Manso, A. B. McIntosh, A. Jedele, K. Hagel, L. Heilborn, Z. Kohley, L. W. May, A. Zarrella, and S. J. Yennello. Detailed characterization of neutron-proton equilibration in dynamically deformed nuclear systems. *Phys. Rev. C*, 95(4):044604, 2017.

[41] Han-Sheng Wang, Jun Xu, Bao-An Li, and Wen-Qing Shen. Reexamining the isospin-relaxation time in intermediate-energy heavy-ion collisions. *Phys. Rev. C*, 98(5):054608, 2018.

[42] R. Bougault et al. Light charged clusters emitted in 32 MeV/nucleon ^{136,124}Xe+^{124,112}Sn reactions: Chemical equilibrium and production of ^{3}He and ^{6}He. *Phys. Rev. C*, 97(2):024612, 2018.

[43] L. W. May et al. Neutron-proton equilibration in 35 MeV/u collisions of 64,70 Zn + 64,70 Zn and 64 Zn, 64 Ni + 64 Zn, 64 Ni quantified using triplicate probes. *Phys. Rev. C*, 98(4):044602, 2018.

[44] Q. Fable et al. Experimental study of isospin transport with Ca40,48+Ca40,48 reactions at 35 MeV/nucleon. *Phys. Rev. C*, 107(1):014604, 2023.

[45] E. De Filippo and A. Pagano. Experimental effects on dynamics and thermodynamics in nuclear reactions on the symmetry energy as seen by the CHIMERA 4π detector. *Eur. Phys. J. A*, 50:32, 2014.

[46] V. Baran, M. Colonna, M. Di Toro, V. Greco, M. Zielinska-Pfabe, and H. H. Wolter. Isospin effects in nuclear fragmentation. *Nucl. Phys. A*, 703:603–632, 2002.

[47] V. Baran, M. Colonna, and M. Di Toro. Neck fragmentation reaction mechanism. *Nucl. Phys. A*, 730:329–354, 2004.

[48] V. Baran, M. Colonna, M. Di Toro, M. Zielinska-Pfabe, and H. H. Wolter. Isospin transport at Fermi energies. *Phys. Rev. C*, 72:064620, 2005.

[49] Maria Colonna, Virgil Baran, and Massimo Di Toro. Theoretical predictions of experimental observables sensitive to the symmetry energy. *Eur. Phys. J. A*, 50:30, 2014.

[50] Maria Colonna. Collision dynamics at medium and relativistic energies. *Progress in Particle and Nuclear Physics*, 113:103775, 2020.

[51] Lie-Wen Chen, C. M. Ko, and Bao-An Li. Light cluster production in intermediate-energy heavy ion collisions induced by neutron rich nuclei. *Nucl. Phys. A*, 729:809–834, 2003.

[52] Yongjia Wang, Chenchen Guo, Qingfeng Li, and Hongfei Zhang. ^{3}H/^{3}He ratio as a probe of the nuclear symmetry energy at sub-saturation densities. *Eur. Phys. J. A*, 51(3):37, 2015.

[53] T. Gaitanos, M. Colonna, M. Di Toro, and H. H. Wolter. Stopping and isospin equilibration in heavy ion collisions. *Phys. Lett. B*, 595:209–215, 2004.

[54] Gao-Chan Yong, Bao-An Li, Lie-Wen Chen, and Xun-Chao Zhang. Triton-He-3 relative and differential flows as probes of the nuclear symmetry energy at supra-saturation densities. *Phys. Rev. C*, 80:044608, 2009.

[55] P. Chomaz and F. Gulminelli. Phase transition in an isospin dependent lattice gas model. *Phys. Lett. B*, 447:221–226, 1999.

[56] S. Albergo, S. Costa, E. Costanzo, and A. Rubbino. Temperature and free-nucleon densities of nuclear matter exploding into light clusters in heavy-ion collisions. *Nuovo Cim. A*, 89:1–28, 1985.

[57] H. S. Xu et al. Isospin fractionation in nuclear multifragmentation. *Phys. Rev. Lett.*, 85:716–719, 2000.

[58] M. A. Famiano, T. Liu, W. G. Lynch, A. M. Rogers, M. B. Tsang, M. S. Wallace, R. J. Charity, S. Komarov, D. G. Sarantites, and L. G. Sobotka. Neutron and Proton Transverse Emission Ratio Measurements and the Density Dependence of the Asymmetry Term of the Nuclear Equation of State. *Phys. Rev. Lett.*, 97:052701, 2006.

[59] S. Nagamiya, M. C. Lemaire, E. Moller, S. Schnetzer, G. Shapiro, H. Steiner, and I. Tanihata. Production of Pions and Light Fragments at Large Angles in High-Energy Nuclear Collisions. *Phys. Rev. C*, 24:971–1009, 1981.

[60] M. Veselsky, R. W. Ibbotson, R. Laforest, E. Ramakrishnan, D. J. Rowland, A. Ruangma, E. M. Winchester, E. Martin, and S. J. Yennello. Isospin dependence of isobaric ratio Y(H-3) / Y(He-3) and its possible statistical interpretation. *Phys. Lett. B*, 497:1–7, 2001.

[61] F. Rami et al. Isospin tracing: A Probe of nonequilibrium in central heavy ion collisions. *Phys. Rev. Lett.*, 84:1120–1123, 2000.

[62] Yu. B. Gurov, L. Yu. Korotkova, S. V. Lapushkin, R. V. Pritula, B. A. Chernyshev, and T. D. Schurenkova. Yields of triton and3He produced by nuclei in reactions of stopped pion absorption. *Bull. Russ. Acad. Sci. Phys.*, 78(11):1112–1116, 2014.

[63] G. Poggi et al. Evidence for collective expansion in light-particle emission following Au+Au collisions at 100, 150 and 250 A·MeV. *Nucl. Phys. A*, 586(4):755–776, 1995.

[64] R Bougault, P Eudes, D Gourio, O Tirel, E Plagnol, C Volant, T Reposeur, CO Bacri, JL Charvet, N Le Neindre, et al. A possible scenario for the time dependence of the multifragmentation process in *xe* + *sn* collisions: an explanation of the ^{3}he puzzle. Technical report, SCAN-9709121, 1997.

[65] T. X. Liu et al. Isospin observables from fragment energy spectra. *Phys. Rev. C*, 86:024605, 2012.

[66] M. A. Lisa et al. Radial flow in Au + Au collisions at E = 0.25-A/GeV - 1.15-A/Gev. *Phys. Rev. Lett.*, 75:2662–2665, 1995.

[67] A Bonasera, M Bruno, CO Dorso, and PF Mastinu. Critical phenomena in nuclear fragmentation. *La Rivista del Nuovo Cimento*, 23:1–101, 2000.

[68] W. Neubert and A. S. Botvina. What is the physics behind the He-3 - He-4 anomaly? *Eur. Phys. J. A*, 7:101–106, 2000.

[69] D. V. Shetty et al. Intermediate mass fragments and isospin dependence in Sn-124, xe-124 + Sn-124, Sn-112 reactions at 28-MeV/nucleon. *Phys. Rev. C*, 68:054605, 2003.

[70] S. Piantelli et al. Isospin transport phenomena for the systems ^{80}Kr+^{40,48}Ca at 35 MeV/nucleon. *Phys. Rev. C*, 103(1):014603, 2021.

[71] W. Reisdorf et al. Systematics of central heavy ion collisions in the 1A GeV regime. *Nucl. Phys. A*, 848:366–427, 2010.

[72] Fenhai Guan et al. A Compact Spectrometer for Heavy Ion Experiments in the Fermi energy regime. *Nucl. Instrum. Meth. A*, 1011:165592, 2021.

[73] Yi-Jie Wang et al. CSHINE for studies of HBT correlation in Heavy Ion Reactions. *Nucl. Sci. Tech.*, 32(1):4, 2021.

[74] Z. Sun, W.-L. Zhan, Z.-Y. Guo, G. Xiao, and J.-X. Li. Ribll, the radioactive ion beam line in lanzhou. *Nuclear Instruments and Methods in Physics Research Section A: Accelerators, Spectrometers, Detectors and Associated Equipment*,

503(3):496–503, 2003.

[75] J.W. Xia, W.L. Zhan, B.W. Wei, Y.J. Yuan, M.T. Song, W.Z. Zhang, X.D. Yang, P. Yuan, D.Q. Gao, H.W. Zhao, X.T. Yang, G.Q. Xiao, K.T. Man, J.R. Dang, X.H. Cai, Y.F. Wang, J.Y. Tang, W.M. Qiao, Y.N. Rao, Y. He, L.Z. Mao, and Z.Z. Zhou. The heavy ion cooler-storage-ring project (hirfl-csr) at lanzhou. *Nuclear Instruments and Methods in Physics Research Section A: Accelerators, Spectrometers, Detectors and Associated Equipment*, 488(1):11–25, 2002.

[76] Fenhai Guan et al. Track recognition for the $\Delta E - E$ telescopes with silicon strip detectors. *Nucl. Instrum. Meth. A*, 1029:166461, 2022.

[77] Xin-Yue Diao et al. Reconstruction of fission events in heavy ion reactions with the compact spectrometer for heavy ion experiment. *Nucl. Sci. Tech.*, 33(4):40, 2022.

[78] Xianglun Wei et al. Development of Parallel Plate Avalanche Counter for heavy ion collision in radioactive ion beam. *Nucl. Eng. Tech.*, 52(3):575–580, 2020.

[79] Dong Guo et al. An FPGA-based trigger system for CSHINE. *Nucl. Sci. Tech.*, 33(12):162, 2022.

[80] Yingxun Zhang, Ning Wang, Qing-Feng Li, Li Ou, Jun-Long Tian, Min Liu, Kai Zhao, Xi-Zhen Wu, and Zhu-Xia Li. Progress of quantum molecular dynamics model and its applications in heavy ion collisions. *Front. Phys. (Beijing)*, 15:54301, 2020.

[81] R. J. Charity et al. Systematics of complex fragment emission in niobium-induced reactions. *Nucl. Phys. A*, 483:371–405, 1988.

[82] R. J. Charity et al. Emission of unstable clusters from hot Yb compound nuclei. *Phys. Rev. C*, 63:024611, 2001.

[83] J. Aichelin et al. Qmd versus buu/vuu. same results from different theories. *Physics Letters B*, 224:34–39, 1989.

[84] J Aichelin. "Quantum" molecular dynamics—a dynamical microscopic n-body approach to investigate fragment formation and the nuclear equation of state in heavy ion collisions. *Physics Reports*, 202(5-6):233–360, 1991.

[85] Ren-Sheng Wang, Li Ou, and Zhi-Gang Xiao. Production of high-energy neutron beam from deuteron breakup. *Nucl. Sci. Tech.*, 33(7):92, 2022.

[86] Li Ou and Zhi-Gang Xiao. Orientation dichroism effect of proton scattering on deformed nuclei. *Chin. Phys. C*, 44(11):114103, 2020.

[87] Xiao Liang, Li Ou, and Zhigang Xiao. New probe to study the symmetry energy at low nuclear density with the deuteron breakup reaction. *Phys. Rev. C*, 101(2):024603, 2020.

[88] Lie-Wen Chen, Che Ming Ko, Bao-An Li, and Jun Xu. Density slope of the nuclear symmetry energy from the neutron skin thickness of heavy nuclei. *Phys. Rev. C*, 82:024321, 2010.

[89] Yingxun Zhang, Zhuxia Li, Chengshuang Zhou, and M. B. Tsang. Effect of isospin-dependent cluster recognition on the observables in heavy ion collisions. *Phys. Rev. C*, 85:051602, May 2012.

[90] Zheng Jiwen, Wu Enjiu, Zhang Chun, Xiao Zhigang, Wang Sufang, Yin Shuzhi, Jin Genming, Tan Jilian, Jin Weiyang, Song Mingtao, et al. Measurement of fission time scale and excitation energy at scission for 25mev/u 40 ar+ 209 bi fission reaction. *Chinese Physics C*, 23(10):946–953, 1999.

[91] H. H. Gutbrod, A. Sandoval, P. J. Johansen, Arthur M. Poskanzer, J. Gosset, W. G. Meyer, G. D. Westfall, and R. Stock. Final State Interactions in the Production of Hydrogen and Helium Isotopes by Relativistic Heavy Ions on Uranium. *Phys. Rev. Lett.*, 37:667–670, 1976.

[92] W. Reisdorf et al. Central collisions of Au on Au at 150, 250 and 400 MeV/nucleon. *Nucl. Phys. A*, 612:493–556, 1997.

[93] H. Xi et al. Examining the cooling of hot nuclei. *Phys. Rev. C*, 57:R462–R465, 1998.

[94] Ad. R. Raduta, E. Bonnet, B. Borderie, N. Le Neindre, S. Piantelli, and M. F. Rivet. Break-up stage restoration in multifragmentation reactions. *Eur. Phys. J. A*, 32:175–182, 2007.

[95] L. G. Sobotka. Simulations of collisions between nuclei at intermediate energy using the Boltzmann-Uehling-Uhlenbeck equation with neutron skin producing potentials. *Phys. Rev. C*, 50:R1272–R1275, 1994.

[96] R. Lionti, V. Baran, M. Colonna, and M. Di Toro. Isospin dynamics in fragmentation reactions at Fermi energies. *Phys. Lett. B*, 625:33, 2005.

[97] V. Baran, M. Colonna, V. Greco, and M. Di Toro. Reaction dynamics with exotic beams. *Phys. Rept.*, 410:335–466, 2005.

[98] D. D. S. Coupland, W. G. Lynch, M. B. Tsang, P. Danielewicz, and Yingxun Zhang. Influence of Transport Variables on Isospin Transport Ratios. *Phys. Rev. C*, 84:054603, 2011.

[99] V. Baran, M. Colonna, M. Di Toro, and R. Zus. From multifragmentation to neck fragmentation: Mass, isospin, and velocity correlations. *Phys. Rev. C*, 85:054611, 2012.

[100] L. G. Sobotka, R. J. Charity, D. K. Agnihotri, W. Gawlikowicz, T. X. Liu, W. Lynch, U. Schroder, J. Toke, and H. S. Xu. Neutron-proton asymmetry of the midvelocity material in an intermediate-energy heavy ion collision. *Phys. Rev. C*, 62:031603, 2000.

[101] S. Piantelli, P. R. Maurenzig, A. Olmi, L. Bardelli, M. Bini, G. Casini, A. Mangiarotti, G. Pasquali, G. Poggi, and A. A. Stefanini. Distinctive features of Coulomb-related emissions in peripheral heavy ion collisions at Fermi energies. *Phys. Rev. C*, 76:061601, 2007.

[102] E. Vient et al. New "3D calorimetry" of hot nuclei. *Phys. Rev. C*, 98(4):044611, 2018.

[103] E. Plagnol et al. Onset of midvelocity emissions in symmetric heavy ion reactions. *Phys. Rev. C*, 61:014606, 2000.

[104] S. Piantelli, L. Bidini, G. Poggi, M. Bini, G. Casini, P. R. Maurenzig, A. Olmi, G. Pasquali, A. A. Stefanini, and N. Taccetti. Intermediate Mass Fragment Emission Pattern in Peripheral Heavy-Ion Collisions at Fermi Energies. *Phys. Rev. Lett.*, 88:052701, 2002.

[105] D. Theriault et al. Neutron to proton ratios of quasiprojectile and midrapidity emission in the Zn-64 + Zn-64 reaction at 45-MeV/nucleon. *Phys. Rev. C*, 74:051602, 2006.

[106] R. Planeta et al. Centrality dependence of isospin effect signatures in Sn-124 + Ni-64 and Sn-112 + Ni-58 reactions. *Phys. Rev. C*, 77:014610, 2008.

[107] Z. Kohley et al. Transverse collective flow and midrapidity emission of isotopically identified light charged particles. *Phys. Rev. C*, 83:044601, 2011.

[108] R. Ogul, A. S. Botvina, M. Bleicher, N. Buyukcizmeci, A. Ergun, H. Imal, Y. Leifels, and W. Trautmann. Isospin compositions of correlated sources in the Fermi energy domain. *Phys. Rev. C*, 107(5):054606, 2023.